Revealing Liquid-Gas Transitions with Finite-Size Scaling in Experimental and Simulation Systems Confined by an External Field - Electronic Supplementary Information

Chong Zha[ab],* Yanshuang Chen[c],* Cheng-Ran Du[d],† Peng Tan[ce],‡ and Yuliang Jin[abf]§
[a] *Institute of Theoretical Physics, Chinese Academy of Sciences, Beijing 100190, China*
[b] *School of Physical Sciences, University of Chinese Academy of Sciences, Beijing 100049, China*
[c] *Department of Physics and State Key Laboratory of Surface Physics, Fudan University, Shanghai, 200438, P. R. China*
[d] *College of Physics, Donghua University, Shanghai, 201620, P. R. China*
[e] *Institute for Nanoelectronic Devices and Quantum Computing, Fudan University, Shanghai, 200438, P. R. China and*
[f] *Wenzhou Institute, University of Chinese Academy of Sciences, Wenzhou, Zhejiang 325000, China*
(Dated: February 9, 2026)

S1. FREE ENERGY OF A CANONICAL ENSEMBLE IN A CONFINING FIELD

We consider a d-dimensional system with a fixed particle number N, at a temperature T, confined by a potential well $U(r)$. Below we use the cluster expansion approach to show that the free energy density of this system, $f = F/N$, depends only on two thermodynamic parameters, $\bar{n} = N/\int e^{-\beta U(r)} d\mathbf{r}$ and T. Note that, due to the confining potential, the pressure $P(r)$ naturally depends on r, but we assume that T is r-independent.

The partition function is

$$Z = \frac{1}{N!\lambda^{Nd}} Z_N, \tag{S1}$$

where

$$Z_N = \int \cdots \int d\mathbf{r}_i \prod_{i=1}^{N} \left[e^{-\beta U(r_i)}\right] \prod_{i<j} \left[f(r_{ij}) + 1\right]. \tag{S2}$$

Here $f(r_{ij}) = e^{-\beta u_{\rm int}(r_{ij})} - 1$ is the Mayer function, $u_{\rm int}(r_{ij})$ the interparticle potential, and $\lambda = 1$ the de Broglie wavelength. Following the standard cluster expansion [1], we can write

$$Z_N = \sum_{\{n_l\}}{}' \prod_l \frac{N! b_l^{n_l}}{n_l!(l!)^{n_l}}, \tag{S3}$$

where $\sum'_{\{n_l\}}$ means a summation over all possible n_l under a constraint $\sum_{l=1}^{N} n_l l = N$. The cluster integral is,

$$b_l = \int \cdots \int d\mathbf{r}_i \prod_{i=1}^{l} \left[e^{-\beta U(r_i)}\right] \sum_{\text{all } l-\text{clusters}} f(r_{ij}) f(r_{mn}) \cdots \tag{S4}$$

As shown in Ref. [1], in the thermodynamic limit,

$$\lim_{N\to\infty} \ln \frac{Z_N}{N!} = \ln T_m, \tag{S5}$$

where T_m is the largest term in the summation of Eq. (S3). To calculate T_m, we use the method of Lagrange multipliers. Using the Stirling formula, we can write a general term in Eq. (S3) as,

$$\ln T(\{n_l\}) = \sum_{l=1}^{N} n_l (\ln b_l - \ln l! - \ln n_l + 1). \tag{S6}$$

* Contributed equally to this work
† chengran.du@dhu.edu.cn
‡ tanpeng@fudan.edu.cn
§ yuliangjin@mail.itp.ac.cn

The largest term satisfies the conditional extreme value equation:

$$\left.\frac{\partial \ln T}{\partial n_l}\right|_{\sum_l n_l l = N} = 0. \tag{S7}$$

For $\mathcal{L} = \ln T - \eta(\sum_l n_l l - N)$, the solution of $\frac{\partial \mathcal{L}}{\partial n_l} = 0$ is

$$\begin{cases} n_l = \dfrac{b_l}{l!} e^{-\eta l}, \\ N = \displaystyle\sum_{l=1}^{N} \frac{b_l}{(l-1)!} e^{-\eta l}. \end{cases} \tag{S8}$$

Denoting $\tilde{b}_l = \frac{b_l}{b_1}$, we have,

$$\sum_{l=1}^{N} \frac{\tilde{b}_l}{(l-1)!} e^{-\eta l} = \bar{n}, \tag{S9}$$

which means that $x \equiv e^{-\eta}$ can be expressed as a function of $\bar{n}$ and $\{\tilde{b}_l\}$ (note that $b_1 = \int d\mathbf{r} e^{-\beta U(r)}$ and $\bar{n} = \frac{N}{b_1}$).

Finally, in the large-N limit,

$$f = \frac{1}{N} \ln \frac{Z_N}{N!} = \frac{1}{N} \ln T_m = \frac{1}{\bar{n}} \sum_{l=1}^{N} \frac{\tilde{b}_l}{l!} x^l - \ln x. \tag{S10}$$

We expect that in this limit, the dimensionless quantity $\tilde{b}_l$ only depends on $\bar{n}$ and T, not on $U(r)$. For example, taking $U(r) = \frac{1}{2} k r^2$, we obtain,

$$\lim_{N\to\infty} \tilde{b}_2 = \frac{2^{1-d/2} S_d}{\bar{n}} \int_0^\infty r^{d-1} f(r) dr, \tag{S11}$$

where S_d is the surface area of a unit sphere in d dimensions. Equation (S11) does not depend on $U(r)$ because in the $N \to \infty$, one has to send $k \to 0$, which gives a final expression that depends on the combination of N and $U(r)$, i.e., $\bar{n}$. Then, according to Eq. (S10),

$$f[N \to \infty, T, U(r)] = f(\bar{n}, T). \tag{S12}$$

Equation (S12) shows that for a system confined by a field, the proper thermodynamic parameters are $\bar{n}$ and T.

S2. EXAMINING THE VALIDITY OF THE FINITE-SIZE SCALING NEAR T_c

As the system approaches the critical point, strong critical fluctuations become dominant, causing the measured gas-liquid interfacial width W no longer reflecting the intrinsic interfacial width. As a result, the apparent interface thickness exhibits a pronounced dependence on the system size, leading to the breakdown of the present method. An example is shown in Fig. S1 for a simulated complex plasma system with Kompaneets interactions at $T = 0.00375$, which is very close to the critical temperature $T_c = 0.0038$. In this regime, the intersections of the rescaled density profiles become slightly smeared out and occur over a range of positions rather than at a single, well-defined point. Although the intersection point becomes somewhat blurred when W depends weakly on N, it is still sufficient to provide an effective criterion for liquid–gas coexistence. The relative distance from the critical point, $(T_c - T)/T_c$, is approximately 0.13. In systems subject to a one-dimensional external potential, where the interface is effectively planar and no curvature-induced suppression of long-wavelength capillary modes is present, critical fluctuations are expected to be stronger. As a consequence, the range of temperatures over which the present method breaks down is likely to be larger than that for systems with curved interfaces. A quantitative assessment of this effect, however, is beyond the scope of the present work. The present approach is therefore restricted to conditions not very close to the critical point.

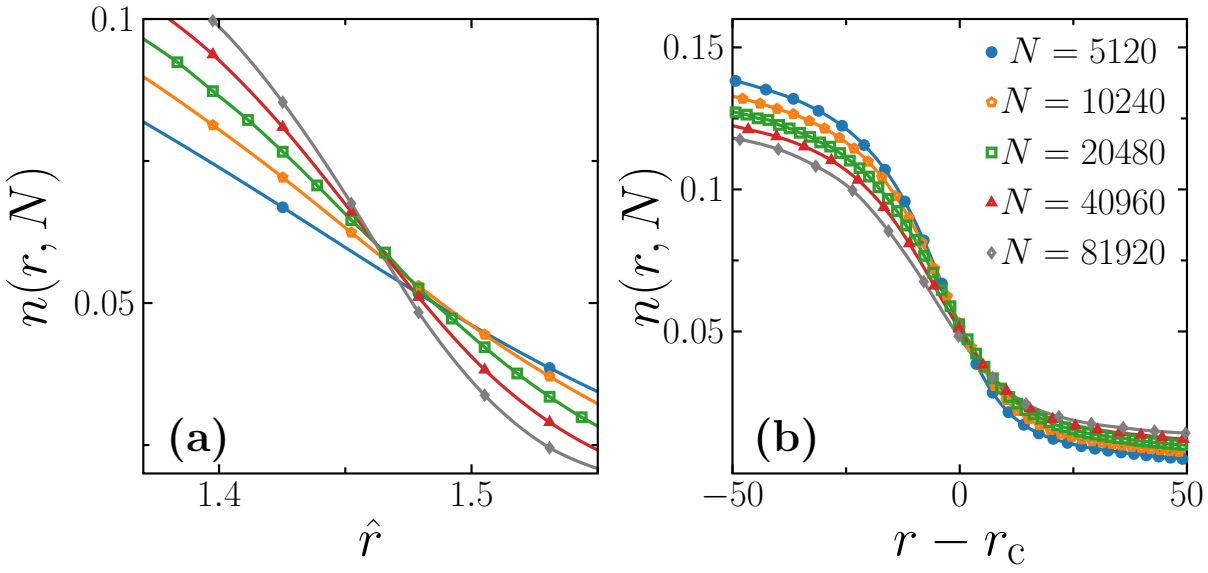

FIG. S1. **Examination of the finite-size scaling near the critical point.** (a) Rescaled density profiles of simulated complex plasma systems with the Kompaneets interaction near T_c. (b) Corresponding density profiles of simulated complex plasma near r_c. The temperature is $T = 0.00375$.

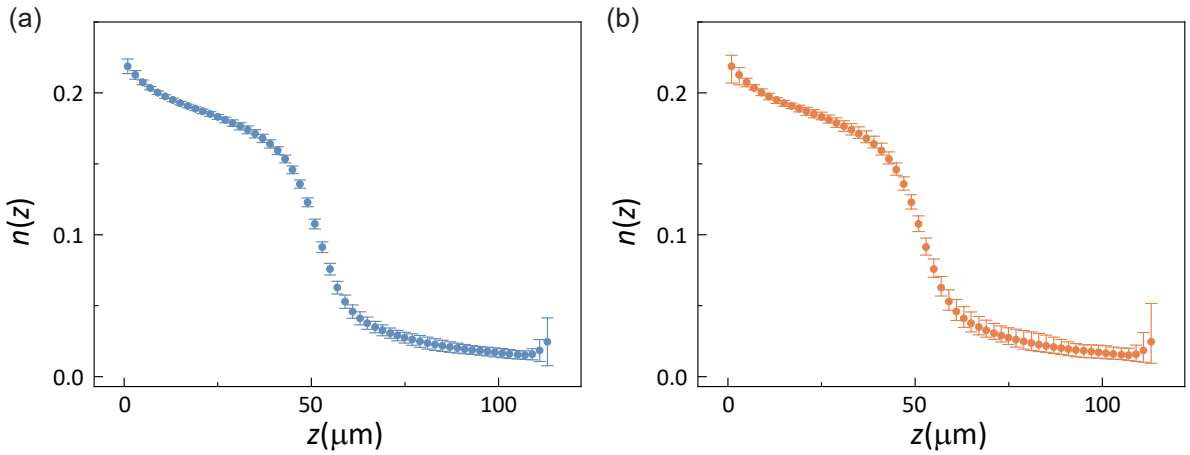

FIG. S2. **The density profile with uncertainty (error bars), measured in experiments.** (a) Error bars represent the standard deviation of the density. (b) Error bars represent the range of density within the slice.

S3. DETERMINATION OF THE INTERSECTION POINT OF DENSITY PROFILES

We first discuss how the uncertainties are estimated for the density profiles measured in our experimental data. The primary sources of uncertainty are: (1) the finite precision in locating individual particles and (2) inherent density fluctuations across different measurement times. To address this, we repeat the measurement of $n(z)$ over several times. At a given height z, the local density $n(z)$ is computed by averaging particle counts within a thin vertical slice $(z - dz, z + dz)$. The uncertainty at z is the standard deviation of $n(z)$ obtained from these repeated measurements. The error bars are small and difficult to display clearly in Fig. 2 of the main text (see Fig. S2).

Next we discuss the statistical significance in the determination of the intersection point. In the main text, we have shown theoretically that the rescaled density profiles collapse when there is no phase transition, while they intersect at a single point when there is a transition. In order to distinguish between the two cases quantitatively in experiments, we design a cost function based on the root mean square error (RMSE) for a cluster of density profile curves. For any two curves $n_i(\hat{z})$ and $n_j(\hat{z})$, we define

$$\Delta n_{ij}(\hat{z}) = n_i(\hat{z}) - n_j(\hat{z}). \tag{S13}$$

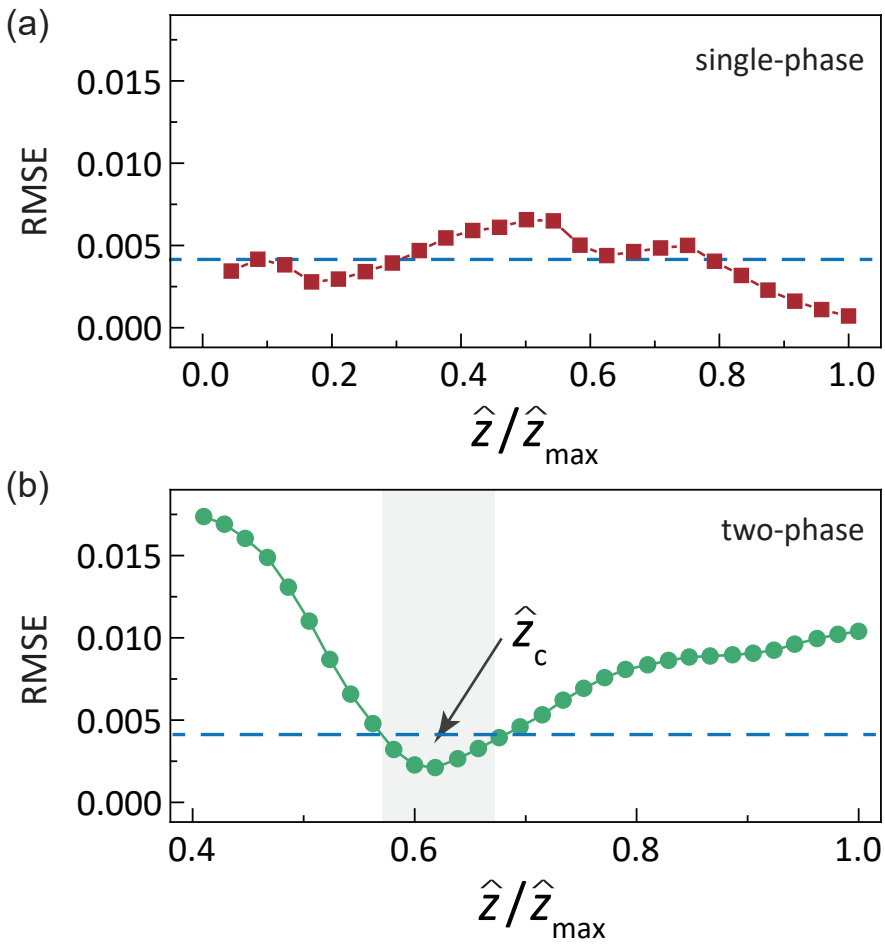

FIG. S3. **RMSE $\Delta(\hat{z})$ for rescaled density profiles obtained in colloidal experiments.** (a) Data for a single-phase system. The dashed line represents $\Delta_{\rm th} = 0.004$. (b) Data for a two-phase system. The locus of the minimum determines $\hat{z}_c$. The part of the data curve below $\Delta_{\rm th}$ provides an estimate of the uncertainty (gray area).

The RMSE $\Delta(\hat{z})$ is:

$$\Delta(\hat{z}) = \left[\frac{2}{M(M-1)} \sum_{i=1}^{M-1} \sum_{j=i+1}^{M} \Delta n_{ij}^2(\hat{z}) \right]^{1/2}, \tag{S14}$$

where M is the total number of compared curves.

Figure S3 displays the data from the colloidal experiments. As shown in Fig. S3(a), for the single-phase system, the value of $\Delta(\hat{z})$ is small, and nearly independent of $\hat{z}$. The average of this curve serves as the "baseline threshold", $\Delta_{\rm th} = 0.004$, for our numerical estimation.

For a two-phase system, $\Delta(\hat{z})$ exhibits a pronounced minimum at the interface position $\hat{z}_c$, providing a clear quantitative signature of intersection (Fig. S3b). In practice, we determine $\hat{z}_c$ by the locus of the minimum. The uncertainty of $\hat{z}_c$ is estimated by comparing the curve to the baseline threshold, $\Delta_{\rm th} = 0.004$ (see Fig. S3b).

S4. EQUILIBRATION CRITERIA

In simulations, we use the mean-squared displacement (MSD) to examine if a system has reached equilibration. In complex plasma simulations, particles are confined in a two-dimensional potential well. In this case, the MSD reaches a constant when the system is in equilibrium (see Fig. S4a). In simulations of the colloidal suspensions, we use periodic boundary conditions at the four-side surfaces. In this case, the MSD is a linear function of time, showing diffusive behavior, when the system has reached equilibration (see Fig. S4b).

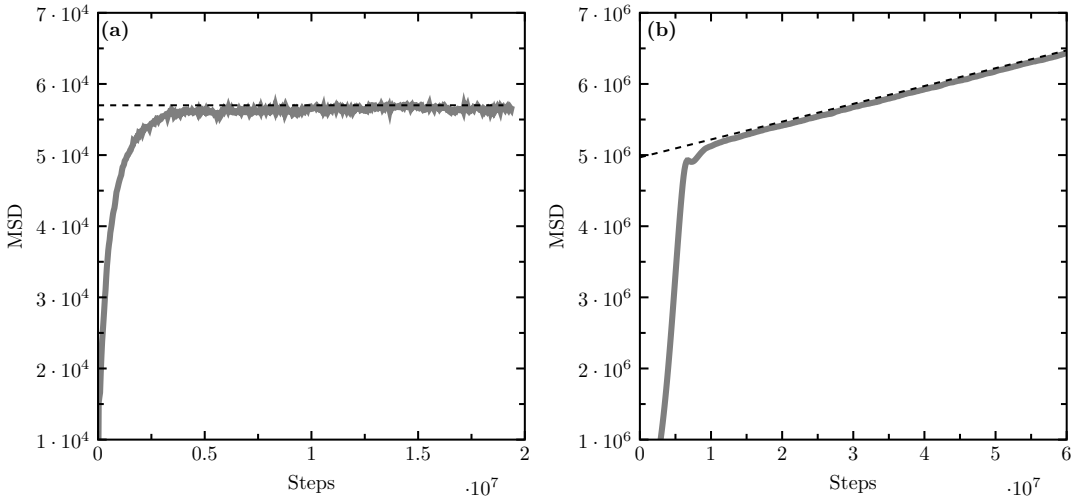

FIG. S4. **Mean-squared displacement (MSD) in simulations.** (**a**) MSD as a function MD time steps for a complex plasma with $N = 10240$ and $T = 0.0031$. (**b**) MSD for a colloidal suspension with $N = 15360$ and $T = 0.11$.

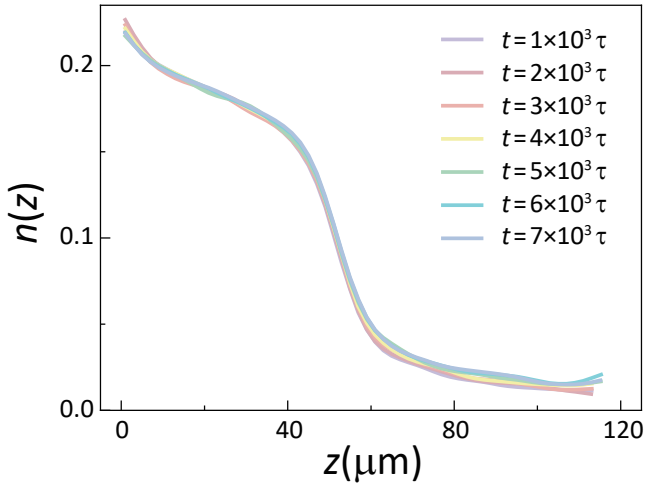

FIG. S5. **The density profiles at different time intervals.** Density profiles measured at different time intervals t, where $t \gg \tau$. Here, $\tau \approx 0.03$ s is the single particle diffusion time in the colloidal system with weak attractive interaction. The superposition of all profiles confirms that the system has reached an equilibrium state.

To verify equilibrium for the colloidal suspensions in experiments, we measure the density profile at time intervals substantially longer than the single-particle relaxation time τ. The profile shows no significant temporal variation, confirming that the system is in equilibrium during our measurements (see Fig. S4).

S5. FITTING THE DENSITY PROFILES

Here we provide quantitative analyses on the shape of density profiles in complex plasmas. We fit the density profiles for Yukawa systems and subcritical Kompaneets systems (see Fig. S6a,b for the fitting curves, and Tables S1 and S2 for the fitting parameters). In the simulated Yukawa system, we employ an ideal-gas density profile combined with a sigmoid function to fit the data:

$$n_{1-\text{phase}}(r) = \frac{\rho_0 e^{-\alpha r^2 - \eta r^4}}{1 + e^{(r-R)/W}}. \tag{S15}$$

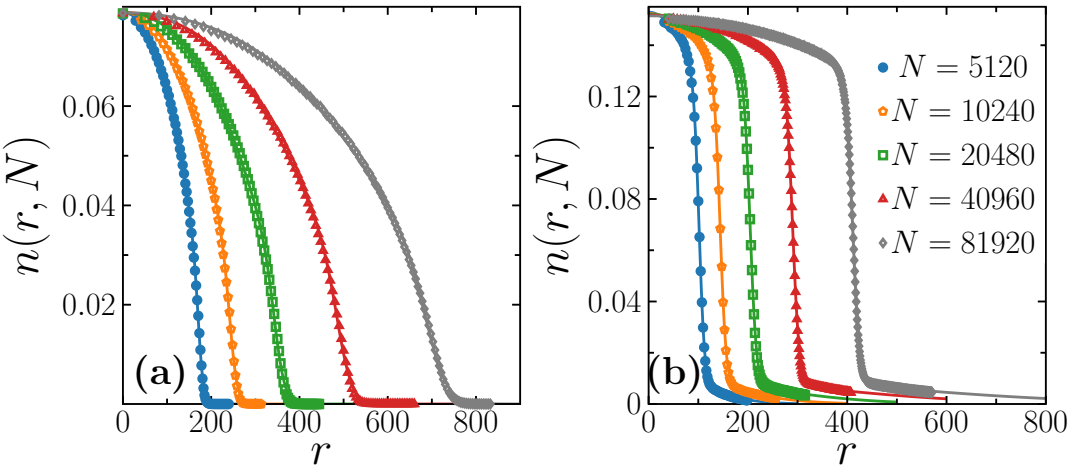

FIG. S6. **Fitting of the density profiles of complex plasmas.** (a) Supercritical systems with the Yukawa interaction at $T = 0.0031$. The fitting model is Eq. (S15). (b) Subcritical systems with the Kompaneets interaction at $T = 0.0031$. The fitting model is Eq. (S17). Please see Table. S1 and S2 for fitting parameters.

This form is modified from the ideal-gas density profile in a Harmonic potential well,

$$n_{\mathrm{IG}}(r) = \rho_0 e^{-\alpha r^2}. \tag{S16}$$

Since no phase separation occurs in the Yukawa case, W in Eq. (S15) does not correspond to a true interfacial width. Instead, W varies strongly with increasing N, indicating that it behaves as an extensive bulk property of the single-phase system. Indeed, the ratios $R/\sqrt{N}$, $W/\sqrt{N}$, α/N, and η/N^2 remain nearly constant for different particle numbers (see Table S1), consistent with the collapse of the density profiles.

For the subcritical Kompaneets systems, the fitting function is,

$$n_{2-\mathrm{phase}}(r) = \frac{(\rho_{\mathrm{L}} - \rho_{\mathrm{g}})e^{-\kappa r^2}}{1 + e^{(r-R)/W}} + \rho_{\mathrm{g}} e^{-\gamma r^2}. \tag{S17}$$

Physically, W in Eq. (S17) characterizes the width of the interface, while R denotes its location. For subcritical Kompaneets systems of different sizes, the width W remains approximately constant, leading to significantly different values of $W/\sqrt{N}$ (see Table S2). This behavior is consistent with the crossing of the corresponding density profiles.

Yukawa systems					
N	ρ_0	α	η	R	W
5120	0.079	1.53×10^{-5}	6.52×10^{-10}	172.85	6.15
10240	0.079	7.31×10^{-6}	1.66×10^{-10}	245.30	8.77
20480	0.079	3.52×10^{-6}	4.28×10^{-11}	347.82	12.20
40960	0.079	1.73×10^{-6}	1.086×10^{-11}	492.35	17.05
81920	0.079	8.71×10^{-7}	2.68×10^{-12}	696.33	24.34

TABLE S1. **Fitting parameters for simulated Yukawa systems.** The fitting function is Eq. (S15).

Kompaneets systems						
N	ρ_{L}	ρ_{g}	κ	γ	R	W
5120	0.142	0.011	1.55×10^{-5}	4.78×10^{-5}	101.95	5.58
10240	0.141	0.011	6.84×10^{-6}	2.33×10^{-5}	144.15	6.02
20480	0.141	0.011	3.27×10^{-6}	1.07×10^{-5}	204.59	6.33
40960	0.141	0.011	1.62×10^{-6}	4.59×10^{-6}	290.07	6.72
81920	0.140	0.012	7.43×10^{-7}	2.68×10^{-6}	410.85	7.04

TABLE S2. **Fitting parameters for simulated Kompaneets systems.** The fitting function is Eq. (S17).

[1] J. Mayer and M. Goeppert, Mayer, statistical mechanics, John Wiley & Sons, New York (1940).